# Performance of large arrays of point absorbing direct-driven wave energy converters

J. Engström, M. Eriksson, M. Göteman, J. Isberg, and M. Leijon

Citation: J. Appl. Phys. **114**, 204502 (2013); doi: 10.1063/1.4833241
View online: http://dx.doi.org/10.1063/1.4833241
View Table of Contents: http://jap.aip.org/resource/1/JAPIAU/v114/i20
Published by the AIP Publishing LLC.

JOURNAL OF APPLIED PHYSICS **114**, 204502 (2013)

# Performance of large arrays of point absorbing direct-driven wave energy converters

J. Engström,[a] M. Eriksson, M. Göteman, J. Isberg, and M. Leijon
*Department of Engineering Sciences, Swedish Centre for Renewable Electric Energy Conversion, Division of Electricity, The Ångström Laboratory, Uppsala University, Box 534, 75121 Uppsala, Sweden*

(Received 11 September 2013; accepted 8 November 2013; published online 22 November 2013)

Future commercial installation of wave energy plants using point absorber technology will require clusters of tens up to several hundred devices, in order to reach a viable electricity production. Interconnected devices also serve the purpose of power smoothing, which is especially important for devices using direct-driven power take off. The scope of this paper is to evaluate a method to optimize wave energy farms in terms of power production, economic viability, and resources. In particular, the paper deals with the power variation in a large array of point-absorbing direct-driven wave energy converters, and the smoothing effect due to the number of devices and their hydrodynamic interactions. A few array geometries are compared and 34 sea states measured at the Lysekil research site at the Swedish west coast are used in the simulations. Potential linear flow theory is used with full hydrodynamic interactions between the buoys. It is shown that the variance in power production depends crucially on the geometry of the array and the number of interacting devices, but not significantly on the energy period of the waves.  [http://dx.doi.org/10.1063/1.4833241]

## I. INTRODUCTION

For large-scale utilization of wave power from the oceans, it is required that a large number of Wave Energy Converters (WECs) operate simultaneously. In particular, this is the case for a WEC concept based on point-absorbers, which consists of large arrays of wave-absorbing units with a spatial extent smaller than the wavelength of the incoming ocean waves. As the individual units in such wave power arrays interact by scattered and radiated waves, the complexity of the modeling increases rapidly with the number of interacting structures, and the numerical simulations are a challenge that call for new methods and theories. Straightforward simulations tend to get very time-consuming when the number of interacting bodies grows.

In certain situations, assumptions can simplify the calculations and enable simulations of a large number of structures. In the point-absorber approximation, the buoys are assumed to be so small that their scattered waves do not interact with the remaining buoys.[1–4] Similarly, in the plane-wave method, the structures are assumed to be too far apart to influence each other by scattered waves.[5–7] The approximate methods work quite well within their assumption limits, but in situations where above approximations do not hold, more general methods are needed. The wave energy devices in focus here are separated by distances small enough for interaction effects to be significant. Therefore, hydrodynamic interactions between the WECs are included in this paper, based on linear potential flow theory.

The interaction of devices in an array is an important area in wave hydrodynamics as well as in electrical engineering: it can lead to a substantial increase or reduction in produced electricity for the array, depending on the geometry, interspacing between the devices and orientation relative to the wave direction and the wave spectrum. On the other hand, the size of the wave energy farm should be minimized to save costs on electrical cable and other material, and to minimize conflict with other interests in the coastal area. In addition, interconnecting wave energy converters in large wave power farms can reduce the fluctuations in power generation, which is a necessity for grid integration.

Earlier works on the power variation in wave energy farms include, e.g., Refs. 8–12. Under the assumption of negligible wave interaction, it was shown that the decrease in standard deviation of the power production for an array of SEAREV devices was strongly connected to the number of devices.[8] More recently, the smoothing effect from a $6 \times 7$ array of Lifesaver WECs was studied and a minimum peak-to-average power of 1.56 was obtained.[12]

In this paper, we study the performance in terms of power production and smoothing for a large array of direct-driven point absorbers of the Uppsala University WEC system. Two array geometries are compared, a rectangular and a double circle segment. In realistic situations, the positions of the WECs are not exact, but tend to drift slightly off their mean positions. These realistic randomized geometries are also taken into consideration in this paper. The model is forced by measured unidirectional time series of wave elevation gathered at the Lysekil wave energy research site off the Swedish west coast.

[a]Author to whom correspondence should be addressed. Electronic mail: jens.engstrom@angstrom.uu.se. Tel.: +46(0)18471 58 18. Fax: +46(0)18471 58 10.

 

## II. THE LYSEKIL WAVE POWER PROJECT

The Uppsala University WEC is of point absorber type with a semi-submerged buoy at the sea surface connected via a line to a direct-driven linear generator at the sea bed, Fig. 1(a). The single stage energy conversion systems results in a wide variation of output voltage, frequency and output power. Therefore, a power conditioning stage becomes necessary for the grid connection of these generators. This is solved by interconnecting several WECs to a common DC bus in a Low Voltage Marine Substation (LVMS). In the future large scale implementation of this system, several LVMS will be connected to one Medium Voltage Marine Substation (MVMS) where the latter will act as a transformer before power is delivered to shore and grid connection point, Fig. 1(b).

Full scale testing of the WEC-system is carried out at the research test site located approximately 2 km offshore south of the town Lysekil, situated between a northern marker (58°11′ 850″N 11° 22′ 460″E) and a southern marker (58° 11′ 630″N 11° 22′ 460″E). It is sheltered by small islands to the north, and a surveillance tower is deployed on the small islet of Klammerskäret to the south. The seabed is fairly level with an average depth of 25 m. A 2.9 km long sea cable connects the WECs and a LVMS to a measurement station on a nearby island. The measurement station and LVMS allows for both linear and non-linear load characteristcs,[13] the LVMS are also prepared for a future grid connection of the WECs. Wave elevation data are collected approximately 50 m from the WEC. Variations in the water level due to tides and air pressure variations are very small at this site and have been neglected in this study. At the test site, 44% of the annual energy flux occurs for sea states with an energy period $T_e$ in the interval 4–7 s and a significant wave height $H_s$ in the interval 1–3 m.[14] For more information on the Uppsala University research site, see, e.g., Leijon *et al.*[15]

## III. THEORY

Ocean waves with amplitudes much smaller than the wave length can with good accuracy be described by potential linear wave theory.[16] This assumes an ideal fluid, i.e., the fluid is incompressible, irrotational, and non-viscous which implies that the velocity potential $\phi$ satisfies the Laplace equation $\nabla^2\phi = 0$. Since the waves are assumed to have small amplitude compared to wave length, the dynamic free surface boundary condition can be linearized.

A device array consists of $N$ wave power devices each in $K$ modes of oscillation. To simplify notation, a combined oscillator index may be defined by

$$j = K(n-1)+k, \quad n = 1,2;..,N, \quad k = 1,2;..,K, \tag{1}$$

where $n$ is the device index and $k$ is the oscillation mode index. The oscillator index is referred to as an array mode of oscillation; there are $KN$ such modes. In our specific case, $N = 32$ and $K = 1$, since we have 32 devices constricted to move in heave only.

Because of the linearity assumption, the hydrodynamic forces associated with each mode of oscillation can be split into two components; the excitation force $F_{e,j}$ and the reaction force $F_{r,j}$ caused by wave radiation.[17] The Fourier transform of the excitation force, $\hat{F}_{e,j}$, is calculated by integrating the pressure over the wet surface $S$ of the buoy according to

$$\hat{F}_{e,j}(\omega) = i\omega\rho\int\int_S \left(\hat{\phi}_0 + \hat{\phi}_d\right) n_j\, dS = \hat{f}_{e,j}(\omega)\hat{\eta}(\omega), \tag{2}$$

where $\rho$ is the density of seawater, $\hat{\phi}_0$, $\hat{\phi}_d$ are the velocity potentials of the incoming wave and the diffracted wave, respectively, $\hat{\eta}(\omega)$ is the Fourier transform of the wave elevation at the surface, and $\hat{f}_{e,j}(\omega)$ is the transfer function for the j:th array mode. Similarly, the radiation force can be written as

$$\hat{F}_{r,j}(\omega) = i\omega\rho\int\int_S \hat{\phi}_r\, n_j\, dS = -\sum_{j'=1}^{MN} \hat{Z}_{j,j'}\hat{\dot{z}}_{j'}, \tag{3}$$

where $\hat{\phi}_r$ is the velocity potential of the radiated waves, $Z$ the radiation impedance, and $z$ the buoy position. With an incoming wave, the equation of motion for each buoy is

$$m_j\ddot{z}_j = F_{e,j} + F_{r,j} - k_s z_j - \gamma\,\dot{z}_j - \rho g\pi a^2 z_j, \tag{4}$$

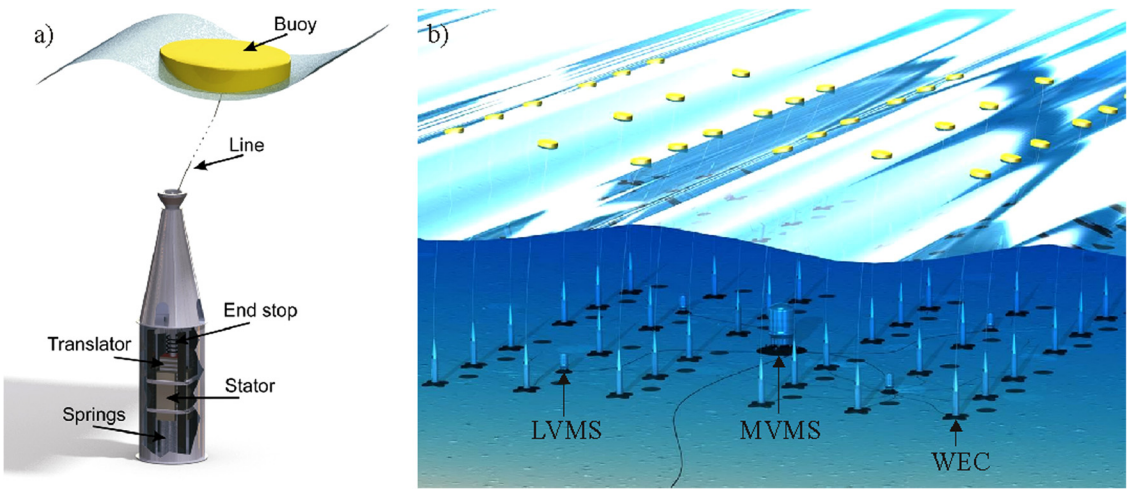


FIG. 1. The Uppsala University WEC in (a). A conceptual sketch of a future commercial scale wave power farm in (b).

where $m$ is the total mass of the moving parts, i.e., the buoy and translator, $k_s$ the spring constant, $\gamma$ is the damping coefficient, and $a$ the buoy radius. The relation between the incident wave and the buoy position is described by $\hat{z}(\omega) = \hat{H}(\omega)\hat{\eta}(\omega)$, where the transfer function $H$ is written as

$$\hat{H}_j(\omega) = \frac{\hat{f}_{e,j}}{-\omega^2\left(m_j + \sum_{j'=1}^{MN}\hat{m}_{a,j,j'}\right) + i\omega\left(\gamma + \sum_{j'=1}^{MN}\hat{R}_{j,j'}\right) + \rho g\pi a^2 + k_s}, \tag{5}$$

where the radiation impedance $Z$, have been divided into radiation resistance $R$ and added mass $m_a$ according to $\hat{Z}_{j,j'} = \hat{R}_{j,j'} + i\omega\hat{m}_{a,j,j'}$.

By taking the inverse Fourier transform of $H$, the buoy position in the time domain is obtained via convolution according to $z(t) = H(t)*\eta(t)$. The absorbed power can be calculated as

$$P_j(t) = \gamma \cdot \dot{z}_j(t)^2. \tag{6}$$

For buoys far from the origin (along the direction of the wave), $\hat{f}_{e,j}(\omega)$, and therefore also $\hat{H}_j(\omega)$, is a rapidly oscillating function of $\omega$, giving rise to severe numerical difficulties when calculating the inverse transform and convolution integrals. To handle this problem, we use a method where the coordinate system is translated to the center of the individual buoys, before computing inverse transforms. This makes the translated version of $\hat{H}_j(\omega)$ a much more slowly varying function of $\omega$. To obtain correct results, the incoming wave also has to be translated by the same distance, but this can be done solely in the time domain, avoiding the corresponding problems associated with rapid oscillations in the translated version of $\hat{\eta}(\omega)$. The translated wave $\eta_d(t)$ at the new origin (for a given buoy) is now calculated from the expression: $\eta_d(t) \equiv \int_{-\infty}^{\infty} K(t-\tau)\eta(\tau)d\tau$, where $K(t) = \frac{\sqrt{g}}{\sqrt{2\pi d}}\left\{\left[\frac{1}{2} + C\left(\sqrt{\frac{g}{4d}}\cdot t\right)\right]\cos\left(\frac{gt^2}{4d}\right) + \left[\frac{1}{2} + S\left(\sqrt{\frac{g}{4d}}\cdot t\right)\right]\sin\left(\frac{gt^2}{4d}\right)\right\}$, $d$ is the distance in the direction of the wave between the new and old origins, and the functions $S$ and $C$ are Fresnel integrals. This method is described in detail in Ref. 18.

To measure the WECs absorption, the Capture Width Ratio (CWR) is defined as

$$CWR_j = \overline{P}_j/2a \cdot J, \tag{7}$$

where the bar denotes average over time and the incident energy transport for waves in waters of infinite depth is $J = \left(\rho g^2/64\pi\right) \cdot T_e H_s^2$. The energy period $T_e$ and the significant wave height $H_s$ are obtained from the spectral moments as $T_e = m_{-1}/m_0$ and $H_s = 4\sqrt{m_0}$. The absorbed power $P$ is the idealized power without any losses. The capture width ratio are calculated for both individual WECs and as a average for the whole arrays, which is described in each figure.

Power production density $\beta$ for the whole array is defined as the average of the total absorbed power of the array divided by the total area of the array according to

$$\beta = \overline{P}_{tot}/Area, \tag{8}$$

where the *Area* are defined as the area of the convex hull, i.e., total enclosed area by line segments of the outermost buoys.

The normalized variance of the produced power is defined as

$$c_{\text{var}} = \frac{\text{var}\,(P_{tot})}{\overline{P}_{tot}{}^2}. \tag{9}$$

## IV. MODELL SPECIFICATION

We illustrate this procedure by comparing capture width ratios and variance for two different array geometries, Figs. 2(a) and 2(b).

The two global geometries are made so that the distance between two adjacent WECs in the circle segment array

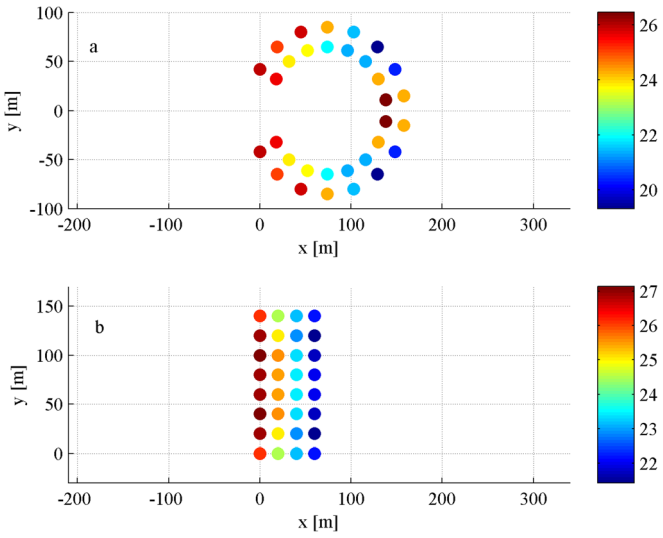


FIG. 2. Global geometry of the double circle segment array in (a) and the rectangular array in (b). Each dot corresponds to a WEC and the colors correspond to respective WECs CWR with the magnitude in percent given by the color bar. The sea state in this case has an energy period of 5.19 s and a significant wave height of 1.07 m. The wave is moving in the positive x-direction.

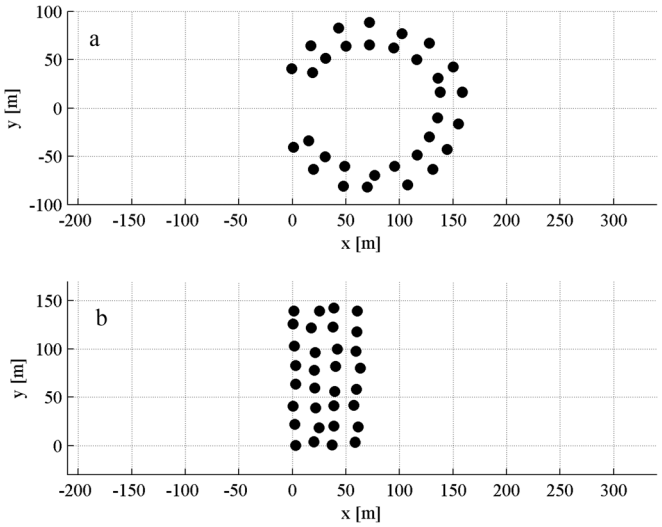


FIG. 3. Randomized circle segment array in (a) and randomized rectangular array in (b).

(excluding the empty area in the center) are approximately the same (20 m) as the distance between two adjacent WECs in the rectangular array. The circle segment array is designed to minimize the cable length from LVMS to the WECs. Furthermore, the opening in the circle segment array serves the purpose as a thought entrance for deployment and maintenance vessels. The circle segment array has a total area of 24 764 $m^2$ and the rectangular array has a total area of 9216 $m^2$. To compare the power production density, Eq. (8), of the circular and rectangular geometries, a larger rectangular array, occupying the same area as the circle segment array, has also been studied. The distance between two adjacent buoys in the larger rectangle is approximately 32 m. In realistic scenarios, the positions of the buoys will not be exact, instead the buoys will tend to drift slightly off their average positions. To account for these realistic wave energy farms, randomized geometries have also been studied in this paper. In these arrays, the coordinates of the buoys are placed on random distances from the original coordinates, with an average of 2.9 m, Figs. 3(a) and 3(b). As we will see, the randomization affects the power smoothing in the rectangular array to a much larger extent than in the circle segment array.

TABLE I. Properties for the 34 sea states used in the calculations ordered with increasing $T_e$.

| $T_e$ (s) | $H_s$ (m) | $T_e$ (s) | $H_s$ (m) |
|---|---|---|---|
| 3.89 | 0.51 | 5.07 | 0.93 |
| 3.95 | 0.49 | 5.16 | 1.39 |
| 4.02 | 0.74 | 5.19 | 1.07 |
| 4.13 | 0.67 | 5.21 | 1.00 |
| 4.21 | 0.62 | 5.24 | 1.12 |
| 4.22 | 0.78 | 5.29 | 0.93 |
| 4.26 | 0.77 | 5.37 | 0.93 |
| 4.35 | 0.80 | 5.47 | 1.03 |
| 4.51 | 0.78 | 5.60 | 1.15 |
| 4.51 | 0.78 | 5.61 | 1.13 |
| 4.53 | 0.79 | 5.76 | 1.03 |
| 4.56 | 0.77 | 6.03 | 1.06 |
| 4.68 | 1.13 | 6.25 | 2.37 |
| 4.85 | 1.31 | 6.54 | 2.15 |
| 4.86 | 0.82 | 6.74 | 2.52 |
| 4.86 | 1.14 | 7.01 | 1.44 |
| 4.94 | 1.27 | 7.34 | 2.36 |

TABLE II. Mechanical characteristics of the WEC.

| | |
|---|---|
| Buoy radius (m) | 2 |
| Buoy draft (m) | 0.5 |
| Translator mass (kg) | 5000 |
| Spring constant (N/m) | 4000 |
| Damping coefficient (Ns/m) | 55 000 |

The model is forced by measured time series of wave elevation collected at the Lysekil test site. For the measurements, a commercial system was used: The Datawell Waverider buoy. The data are obtained at a sampling rate of 2.56 Hz. 34 time series are used that range from $3.89 \langle T_e \rangle 7.34$ and $0.49 \langle H_s \rangle 2.52$, Table I. The wave data cover the predominant sea state at the Lysekil test site and the Swedish west coast.

The WEC in the model models the Lysekil concept WEC which is of point absorber type with a semi-submerged cylinder connected via a line to a direct-driven linear generator. The translator is connected to a retraction spring at the bottom. The generator is modelled to lowest order, with unconstrained stroke length and linear load. The load corresponds to a resistive dump load which is the simplest load characteristics used in the Lysekil project. The WEC is modelled as being rigid and the high translator mass and retraction spring prevent any slack in the line. The model is also constricted to move in heave only. The mechanical characteristics of the WEC in the model are given in Table II. All WECs in the simulation share the same mechanical characteristics.

## V. RESULTS

The shadowing effect of the buoys can clearly be seen in Figs. 2(a) and 2(b), with the non-shadowed WECs receiving the highest CWR. The largest difference can be found in Fig. 2(a), where the CWR ranges from 20% to 26%. From Figs. 2(a) and 2(b), it is also clear that the central WECs of each row receive positive feedback from the surrounding WECs; this pattern is particularly evident in rows 1 and 2 of Fig. 2(b). For a single isolated WEC, the CWR for this specific sea state is 25%, thus a substantial number of WECs in the array achieves a higher CWR than had they been isolated. However, the mean value for the CWR in Fig. 2(a) is 23.5% and in Fig. 2(b) 24.2%, showing that the positive gain in CWR for some WECs is less than the loss in CWR due to the shadowing effect for the rest of the WECs.

The clear trend in Fig. 4(a) is that the CWR reaches its highest values for the lowest energy period and decreases with increasing energy period. This feature was also seen in the experimental data from the three WEC array in Rahm *et al.*[19] The rectangular array and the single WEC reach a slightly higher CWR than the circle-segment array for all sea states but the difference is small.

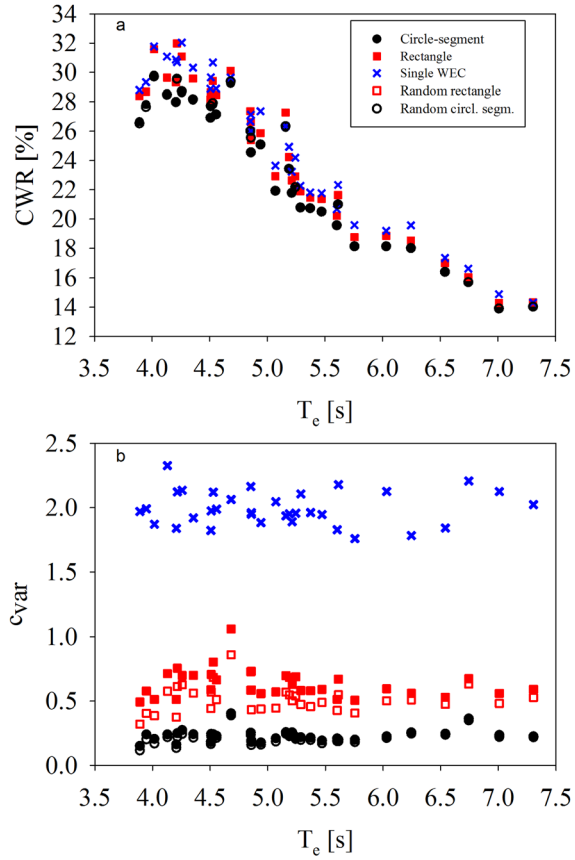


FIG. 4. Average CWR as a function of $T_e$ in (a) and $c_{var}$ as a function of $T_e$ in (b). Black dots correspond to the circle-segment array with 32 WECs, red squares to the rectangular array with 32 WECs, and blue dots represent a single isolated WEC. Non-filled dots and squares correspond to rectangular and circle-segment arrays with randomized WECs. The average is taken over the 32 WECs.

Figure 4(b) shows a large scattering for the variance as a function of energy period, the variance ranges from 0.15 to 0.41 with an average of 0.23 for the circle-segment array and between 0.49 and 1.06 with an average of 0.64 for the rectangular array. For the single isolated WEC, the variance is scattered between 1.84 and 2.33 with an average of 2. It should be noted that for the rectangular array, waves traveling in the x-direction is the worst case scenario. With waves entering with a 45° angle, the variance should be lower. This effect is also illustrated in Fig. 4(b), where the variance in power production of the rectangular geometry is significantly decreased if the buoy positions are randomized. However, the variance is still substantially higher than the variance for the circle segment array. The same procedure was performed for the circle segment array, Fig. 4(b), but the results overwrite each other indicating that a minimum in variance might have been reached for 32 WECs.

The average of the variance for the larger rectangular geometry is 0.54, hence less than the smaller rectangular array, but much larger than the circular one, as depicted in Fig. 5. This shows that the increased distance between the WECs has less importance on the variance than the WECs individual position. For clarity, the results for the larger rectangular array have not been included in Fig. 4(b).

The capacity of a single WEC is often measured in capture width. When discussing full wave energy farms, it is more interesting to know how effective the system is in comparison to the spatial area the farm occupies and this is shown in Fig. 5.

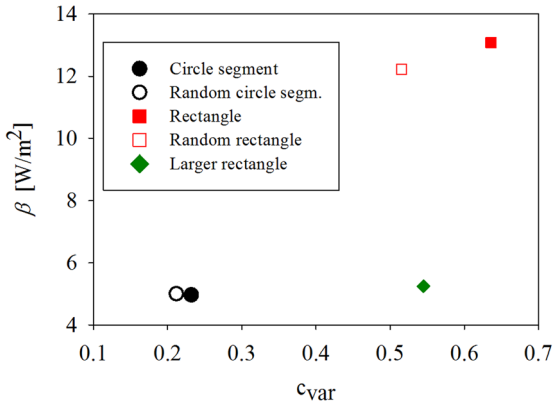


FIG. 5. Average power production density versus average normalized variance. The average is taken over the 34 sea states in Table I.

In the cases studied here, the average power production density $\beta$ is 5 W/m$^2$ for the circle segment and 13 W/m$^2$ for the rectangular array, Fig. 5. Thus, the rectangular array is more than 2 times more effective per square meter due to a more effective use of ocean surface. The larger rectangle shares the same power production density as the circle segment. This loss in power production per square meter should be weighed against the difference in variance (i.e., power quality) which is especially evident when comparing the circle segment with the large rectangle in Fig. 5.

## VI. DISCUSSION AND CONCLUSION

Not surprisingly, the shadowing effect of the buoys is clearly evident, with the non-shadowed WECs having the highest CWR. More interesting is that the central WECs of each row receive a noticeable positive feedback from the surrounding WECs and this pattern compensates, to some extent, for the loss in CWR for the shadowed WECs. The CWR for both the circular and rectangular arrays as a function of energy period follows the values for the single WEC.

The most interesting trend for the normalized variance is that the rectangular array has a much higher variance in power production than the circle-segment array, roughly three times higher on average. Even in randomized geometries, where the coordinates of the buoys are not on exact lattices but instead are placed randomly slightly off the regular lattice points, the difference between the two geometries is still large. Further, the lowest variance for the circle-segment array, 0.15 is roughly a 13th of the average variance for the single WEC; the interaction between the devices provides a power smoothing which is crucial for the commercial installation of wave power farms.

In this paper, the variance of the power production in wave farms has been studied as a function of farm geometry, mainly focusing on the difference between circular and rectangular arrays. The power smoothing as a function of the distance between the buoys will be studied in greater detail in a separate paper.

In terms of produced power per square meter, the rectangular array is most efficient, but when comparing the

circle-segment array to the larger rectangular array, which has the same area as the circle-segment array, Fig. 5, they are more or less equal, since the circle-segment array has a large dead space in the center. However, this dead space should be taken into account when studying the whole system since it will be a prohibited area, while on the other hand, the dead space might be a necessity for deployments and maintenance, which needs to be taken into consideration for future commercial installations. Further, when calculating the power production density for several arrays, i.e., a full farm, one should also include the dead space between the arrays since it will be a prohibited area for most other stakeholders of the sea. For a more industrial approach, an even better measurement might be to calculate the farms production in comparison m/sea cable, since this will be one of the major installation costs. This will be included in a future paper that will study this wave energy conversion system in the MW range with a more realistic electric system.

## ACKNOWLEDGMENTS

This project was supported by the Swedish Energy Agency, Uppsala University, Standup for energy-wave and Carl Tryggers Stiftelse. Magnus Wibling at Seabased Industry AB is thanked for sharing the idea of the circle segment array.

[1]K. Budal, "Theory for absorption of wave power by a system of interacting bodies," J. Ship Res. **21**, 248–253 (1977).
[2]D. Evans, *Some Analytic Results for Two- and Three-Dimensional Wave Energy Absorbers. Power from Sea Waves* (Academic Press, 1980), pp. 213–249.
[3]J. Falnes, "Radiation impedance matrix and optimum power absorption for interacting oscillators in surface waves," Appl. Ocean. Res. **2**, 75–80 (1980).
[4]J. Falnes, "Wave-power absorption by an array of attenuators oscillating with unconstrained amplitudes," Appl. Ocean. Res. **6**(1), 16–22 (1984).
[5]J. Simon, "Multiple scattering in arrays of axisymmetric wave-energy devices. Part 1: A matrix method using a plane-wave approximation," J. Fluid Mech. **120**, 1–25 (1982).
[6]P. McIver and D. Evans, "Approximation of wave forces on cylinder arrays," Appl. Ocean. Res. **6**, 101–107 (1984).
[7]P. McIver, "Wave forces on arrays of floating bodies," J. Eng. Math. **18**, 273–285 (1984).
[8]J. Tissandier, A. Babarit, and A. H. Clément, "Study of the smoothing effect on the power production in an array of SEAREV wave energy converters," in Proceedings of the 18th International Offshore and Polar Engineering Conference, Vancouver, BC, Canada, 6–11 July 2008.
[9]J. Cruz, R. Sykes, P. Siddorn, and R. Eatock Taylor, "Wave farm design: Preliminary studies on the influences of wave climate, array layout and farm control," in Proceedings of the 8th European Wave and Tidal Energy Conference, Uppsala, Sweden, 2009.
[10]D. Kavanagh, A. Keane, and D. Flynn, "Challenges posed by the integration of wave power onto the Irish power system," in Proceedings of the 9th European Wave and Tidal Energy Conference, Southampton, UK, 5–9 September 2011.
[11]A. Blavette, D. L. O'Sullivan, A. W. Lewis, and M. G. Egan, "Impact of a wave farm on its local grid: Voltage limits, flicker level and power fluctuations," in Proceedings of the OCEANS, Yeosu, 21–24 May (2012), pp. 1–9.
[12]J. Sjolte, G. Tjensvoll, and M. Molinas, "Power collection from wave energy farms," Appl. Sci. **3**, 420–436 (2013).
[13]C. Boström, Ph.D. dissertation, Uppsala University, Uppsala, Sweden, 2011.
[14]R. Waters, J. Engström, J. Isberg, and M. Leijon, "Wave climate off the Swedish west coast," Renewable Energy **34**(6), 1600–1606 (2009).
[15]M. Leijon, R. Waters, M. Rahm, O. Svensson, C. Boström, E. Strömstedt, J. Engström, S. Tyrberg, A. Savin, H. Gravråkmo, H. Bernhoff, J. Sundberg, J. Isberg, O. Ågren, O. Danielsson, M. Eriksson, E. Lejerskog, B. Bolund, S. Gustafsson, and K. Thorburn, "Catch the wave to electricity: The conversion of wave motion to electricity using a grid-oriented approach," IEEE Power Energy Mag. **7**(1), 50–54 (2009).
[16]J. J. Stoker, *Water Waves: The Mathematical Theory with Applications* (Wiley Classics Library Edition, New York, 1992).
[17]J. Falnes, *Ocean Waves and Oscillating Systems* (Cambridge University Press, Cambridge, 2002), pp. 1–275.
[18]J. Isberg, J. Engström, M. Eriksson, and M. Leijon, "Numerically efficient hydrodynamic simulation of large arrays of point absorbers," Appl. Phys. Lett. (unpublished).
[19]M. Rahm, O. Svensson, C. Boström, R. Waters, and M. Leijon, "Experimental results from the operation of aggregated wave energy converters," IET Renewable Power Gener. **6**(3), 149–160 (2012).